THE ASTROPHYSICAL JOURNAL, 455:524–535, 1995 December 20

WHEELS OF FIRE. I. MASSIVE STAR FORMATION IN THE CARTWHEEL RING GALAXY

JAMES L. HIGDON[1]
National Radio Astronomy Observatory,[2] Array Operations Center, 1003 Lopezville Road, Socorro, NM 87801
Received 1994 November 15; accepted 1995 June 27

ABSTRACT

Hα CCD imaging is used to map the distribution and intensity of massive star formation (MSF) in the Cartwheel ring galaxy. Line emission is restricted to the outer ring, with upper limits comparable to the disks of early-type galaxies found in the spokes, disk, inner ring, and nucleus. Systematic variations in Hα surface brightness are detected around the ring, with 80% of the total line luminosity ($L_{H\alpha} = 7.4 \times 10^{42}$ ergs s^{-1}, corrected for $A_V = 2.1$) originating in one quadrant. The 29 identified H II region complexes of the ring are characterized by very large Hα luminosities and equivalent widths. In contrast to Hα, the outer ring is faint in red continuum and shows only small azimuthal variations in surface brightness. The systematic variation in line emission around the ring, high star formation rates, and low H II region abundances are evidence that the ring acts to both organize the interstellar medium *and* directly trigger MSF. Faint H II region complexes are found in advance of the outer ring and appear to be spawned by shocks and supernovae from nearby giant H II regions.

The overall distribution of MSF points to a small impact parameter collision with one of the three companion galaxies. The lack of Hα emission from the Cartwheel's inner ring and spokes suggests that they are gas poor. The observed azimuthal variations in $L_{H\alpha}$ and $EW_{H\alpha}$ in the outer ring are most simply explained by systematic changes in age or initial mass function.

Subject headings: galaxies: individual (Cartwheel) — galaxies: starburst — galaxies: stellar content — H II regions

1. INTRODUCTION

Ring galaxies result from the passage of a compact companion galaxy through the disk of a spiral galaxy along its rotation axis (Lynds & Toomre 1976; Theys & Spiegel 1977). For small impact parameters, the collision generates a radially propagating ring-shaped structure in the disk in which the orbits of stellar and gaseous material crowd together. Larger impact parameter collisions produce crescent-shaped rings with an off-centered remnant nucleus. In both cases, the orbit crowding can lead to large increases in the density of stars and gas in the rings at the expense of extended regions throughout the disk. These systems are of particular interest, as the rings may support extended starburst activity. Evidence for elevated star formation rates (SFRs) in ring galaxies is found in their blue optical colors and large far-infrared (FIR) luminosities (Theys & Spiegel 1976; Appleton & Struck-Marcell 1987a). Spectroscopic studies confirm that the rings can possess highly luminous H II regions (Fosbury & Hawarden 1977, hereafter FH; Few, Madore, & Arp 1982; Taylor & Atherton 1984; Jeske 1986). Ring galaxies offer a number of advantages for the study of the starburst phenomenon, including a clear star formation trigger, lower levels of extinction and background emission compared with the more common nuclear starbursts, and the ability to resolve structure in the rings themselves. Because of their symmetry, numerical simulations can be significantly simplified (Struck-Marcell & Higdon 1993). Moreover, the development of large differences in surface density between the ring and disk make these systems promising test cases for gas density threshold models of star formation (e.g., Kennicutt 1989).

This paper presents an Hα imaging study of the Cartwheel ring galaxy, with the goal of determining the intensity and distribution of massive star formation (MSF) over the entire galaxy, as well as basic properties of its H II region population. The Cartwheel was chosen for this investigation because it is one of the largest ring galaxies in both physical ($D_{ring} = 33$ kpc; $H_0 = 100$ km s^{-1} Mpc^{-1}) and angular (80″ × 55″) size and is the most symmetric example of this class. Additional properties of the galaxy are listed in Table 1. Most importantly, the outer ring is known to possess highly luminous star-forming regions (FH). Figure 1 shows an image of the Cartwheel in blue light obtained with the CTIO 4 m by V. Blanco. A wealth of structure is apparent, including a bright inner ring and bar, plus the numerous "spokes" that appear to connect the inner and outer rings. FH found no line emission within 6″ × 3″ apertures placed on the nucleus, inner ring, and one spoke, however. Three companion galaxies are visible in Figure 1 within 3′ of the Cartwheel along the ring's projected minor axis and have been labeled G1, G2, and G3. All three have systemic velocities within 400 km s^{-1} of the Cartwheel's, and therefore they are candidates for the intruder. For convenience the four galaxies will be referred to as the Cartwheel Group.

The primary questions to be addressed in this work are as follows: (1) What is the global distribution of MSF? FH's search will be extended to the entire galaxy, including the network of spokes, which recent numerical simulations suggest are gas rich and capable of supporting detectable levels of MSF (Hernquist & Weil 1993). (2) What role do the rings play in star formation? Is there evidence for the direct triggering of MSF, or do they act primarily to organize the galaxy's interstellar medium (ISM) for spontaneous star formation pro-

[1] NRAO Jansky Fellow.
[2] The National Radio Astronomy Observatory is operated by Associated Universities Inc., under a cooperative agreement with the National Science Foundation.

TABLE 1

PHYSICAL PROPERTIES OF THE CARTWHEEL

Parameter	Value
Right Ascension[a]	$00^h35^m14^s.31$
Declination	$-33°59'29''$
l, b[b]	$326°.6, -82°.7$
Systemic Velocity[c]	9089 ± 8 km s^{-1}
Distance[d]	91 Mpc
Outer Ring Diameter	$80'' \times 55''$, 33×24 kpc
Inner Ring Diameter	$16'' \times 10''$, 7×4 kpc
M_B[e]	-20.94
L_B	$3.7 \times 10^{10}\ L_\odot$
L_{FIR}	$1.0 \times 10^{10}\ L_\odot$
L_{FIR}/L_B	0.3
Oxygen Abundance[f]	8.0

[a] Epoch 1950.0 position of the ring nucleus.
[b] From de Vaucouleurs et al. 1991.
[c] Based on H I analysis (Higdon 1995).
[d] Assuming $H_0 = 100$ km s^{-1} Mpc^{-1}.
[e] Absolute B magnitude corrected for 0.21 mag of Galactic extinction. No correction for inclination.
[f] Mean 12 + log (O/H) for CW 17 and 24 (FH).

cesses? Does the ring's stellar amplitude correlate with the intensity of MSF? (3) How do the emission properties of the Cartwheel's star-forming regions compare with those found in more normal galaxies? And do they vary from one part of the galaxy to another in a systematic way? Subsequent papers will deal with the Cartwheel's broadband optical emission, as well as the properties of its atomic and molecular gas components.

The outline of this paper is as follows: The observations and data reduction are briefly described in § 2. This is followed in § 3 by discussions of the Hα and red continuum morphology of the Cartwheel, and the emission properties of the massive star-forming regions. The implications of these results for the process of MSF in the galaxy are discussed in § 4. Concluding remarks are presented in § 5.

2. OBSERVATIONS, REDUCTION, AND ANALYSIS

Emission-line and continuum maps of the Cartwheel Group were made on 1991 August 16, 18, and 19 with the 0.76 m telescope of the McDonald Observatory. The imaging array was a Tektronics 512 × 512 CCD situated at the f/13.9 Cassegrain focus. The 27 μm pixel separation provided an image scale of 0".52 pixel^{-1} and a field of view large enough to include all four galaxies in a single frame. Readout noise and gain were determined to be $10.3e^-$ and $6.5e^-$ ADU^{-1}. The redshifted Hα line was isolated using an interference filter ($\Delta\lambda = 21$ Å FWHM) centered at 6761 Å. Line-free continuum was measured using a 150 Å FWHM filter centered at 6570 Å. Integrations totaling 4200 and 2400 s were made in the line and continuum filters, respectively. The basic reduction of the individual galaxy frames was routine. The seeing over the three nights was quite good considering the large air masses involved ($X > 2.0$). A point-spread function of 1".7 FWHM was determined through Gaussian fits to stars in the processed images. At the assumed distance of 91 Mpc, this corresponds to a spatial resolution of 750 pc. Using field stars and the line-free companion G2 to normalize the continuum, the final 6570 Å image was subtracted from the line + continuum image, producing a map of the Hα emission in the Cartwheel Group.

As none of the nights were photometric, the Hα calibration was bootstrapped using emission line fluxes measured within $6'' \times 3''$ apertures centered on the brightest star-forming complexes of the outer ring (regions "A" and "B" in FH). Because of the television aperture viewing system used by FH, there was little uncertainty in where the spectra were obtained. For each aperture, $F_{H\alpha}$ was derived from $F_{H\beta}$ assuming case B intrinsic line ratios and FH's determination of reddening. A direct $F_{H\alpha}$ measurement for region "A" was provided by Jeske (1986). These fluxes were combined with simulated aperture photometry in the emission-line map to determine the ADU $- F_{H\alpha}$ conversion. The individual conversion factors differed by ~10%, which can be attributed to small uncertainties in the aperture positions. The 6570 Å map was calibrated using a Cousins R-band ($\lambda_{eff} = 6400$ Å; Bessel 1979) CCD image of the Cartwheel Group from a previous run. The average red continuum flux over the R filter's passband was determined for the Hα-free companion galaxy G2 using simulated aperture photometry. This value was then used to derive the ADU $- F_{6570\ Å}$ conversion factor. In light of the good agreement between the spectrophotometry of the Cartwheel's brightest H II region complex by FH and Jeske (1986) and the ADU $- F_{H\alpha}$ conversion factors derived for the prominent star-forming regions, it is believed that the calibration is accurate to ~10%. As a final consistency check, the Cartwheel's integrated Hα equivalent width ($EW_{H\alpha\ Å}$, the ratio $F_{H\alpha}/F_{6570\ Å}$) determined using the above calibration was compared with a value derived by multiplying the ratio of the summed counts from the galaxy in the line and continuum maps by the line filter FWHM (cf. Kennicutt et al. 1987). The two maps had first been scaled to give identical summed counts from field stars. This second method provides a measure of $EW_{H\alpha}$ independent of the absolute flux calibration. The two values differed by 12%, which is within the expected uncertainty.

The calibrated Hα and continuum maps of the Cartwheel Group are shown in Figures 2*a* and 2*b*. Subimages showing line and continuum emission from the ring galaxy are presented in Figures 2*c* and 2*d*. Small seeing differences between the line and continuum maps are responsible for the residual emission from the foreground star on the western edge of the ring and the bright core of companion G2. Much weaker residual emission is associated with the Cartwheel's nucleus. Since FH found no traces of Hα here, this is also attributed to small point-spread differences. To better quantify variations in line and continuum emission around the ring, averaged azimuthal profiles were derived using the maps. The mean and 1 σ uncertainty were computed within 10° sectors of a 7" wide elliptical annulus fit to the outer ring. Only pixels 3 σ above the noise were included in the calculations. Similarly, azimuthally averaged radial profiles were derived in both Hα and red continuum to better measure low levels of emission between the two rings and to compare properties of the two rings. Line and continuum fluxes from individual H II region complexes were obtained by summing all pixels within interactively defined regions above the 3 σ noise level. Wherever possible, the background line or continuum emission was estimated and subtracted from the H II region fluxes.

3. RESULTS

3.1. *The Intensity and Distribution of MSF*

Using Figure 2*c*, the integrated Hα flux from the Cartwheel was found to be 1.7×10^{-12} ergs s^{-1} cm^{-2}. At the assumed distance of 91 Mpc, this corresponds to $L_{H\alpha} = 1.7 \times 10^{42}$ ergs s^{-1}, with no extinction correction. An average extinction of $A_V = 2.1$ mag was measured in two ring H II regions (FH;

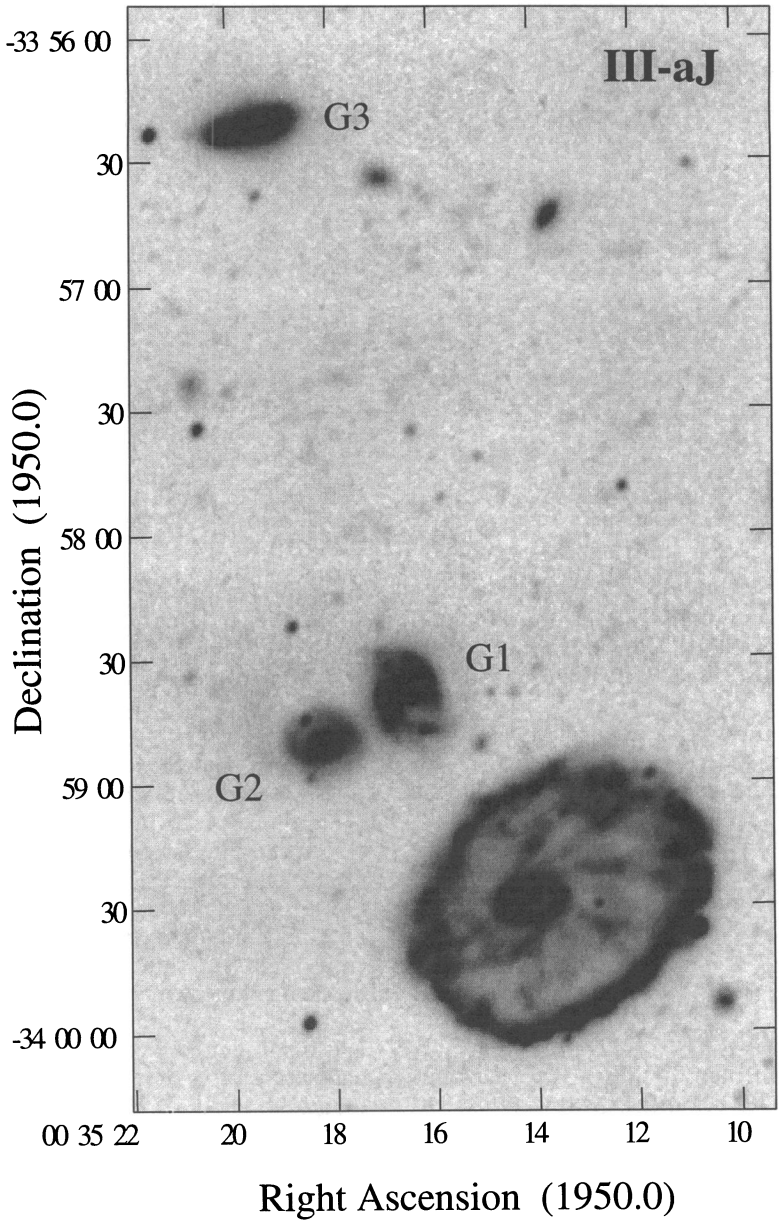

FIG. 1.—Digitized CTIO 4 m prime focus plate obtained by V. Blanco showing the four galaxies of the Cartwheel Group (III aJ + GG385 filter; $\lambda_{\rm eff}$ = 4400 Å)

Jeske 1986). Adopting the reddening law of Savage & Mathis (1979), the corresponding $A_{\rm H\alpha}$ is 1.6. Taking this value to be representative of the outer ring, the extinction-corrected Hα luminosity of the Cartwheel becomes 7.4×10^{42} ergs s^{-1}. In Kennicutt's (1983) list of 115 nearby galaxies, the giant Sc spiral NGC 2276 possessed the largest Hα luminosity ($L_{\rm H\alpha} = 5.6 \times 10^{41}$ ergs s^{-1}, corrected for extinction and scaled to the same Hubble constant). The Cartwheel's $L_{\rm H\alpha}$ exceeds this by more than an order of magnitude. Most striking is the fact that MSF is completely restricted to the narrow outer ring. There is no evidence of H II regions *anywhere* in the Cartwheel's nucleus, bar, inner ring, disk, or spokes above $L_{\rm H\alpha} = 3.0 \times 10^{39}$ ergs s^{-1} (3 σ), a value roughly 15% the Hα luminosity of 30 Doradus (Kennicutt, Edgar, & Hodge 1989). An Hα surface brightness upper limit of 2.6×10^{31} ergs s^{-1} pc^{-2} (3 σ) was set using a smoothed version of Figure 2*c* (5″ FWHM Gaussian kernel). This corresponds to a level less than half the mean Hα surface brightness in the faint interarm region of M51 (Rand 1992).

Line emission varies systematically with position angle (ϕ) around the ring, as the averaged azimuthal Hα profile in Figure 3*a* shows. MSF is strongly peaked over $\phi = 120°$–$250°$. Eighty percent of the Cartwheel's line emission is concentrated in this ring quadrant (southern quadrant). A smaller and fainter arc of enhanced line emission is seen from $\phi = 0°$–$70°$ (northeast quadrant). Around the ring, Hα emission is seen broken up into numerous star-forming complexes, though a faint unresolved component is also present. At least some Hα emission is observed in all parts of the ring. Interesting structure can be seen in the faint Hα emission in several regions of

1995ApJ...455..524H

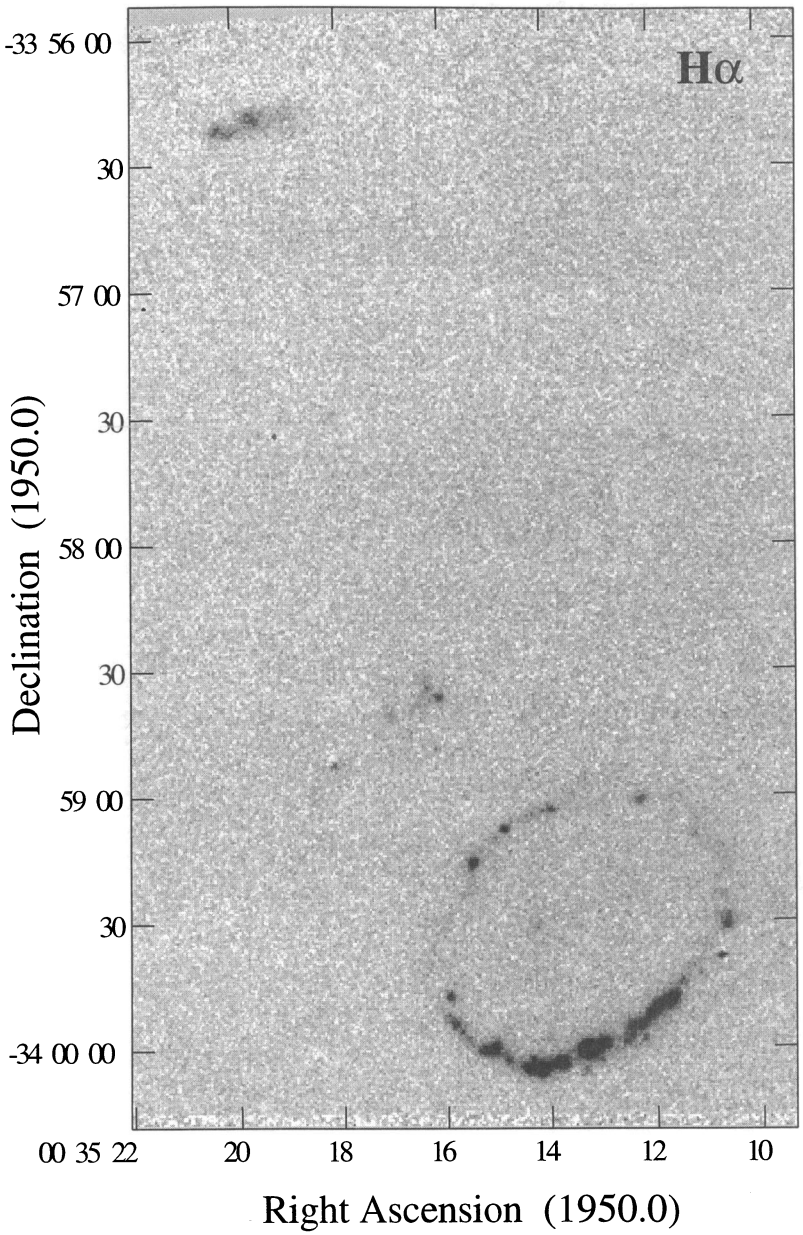

FIG. 2a

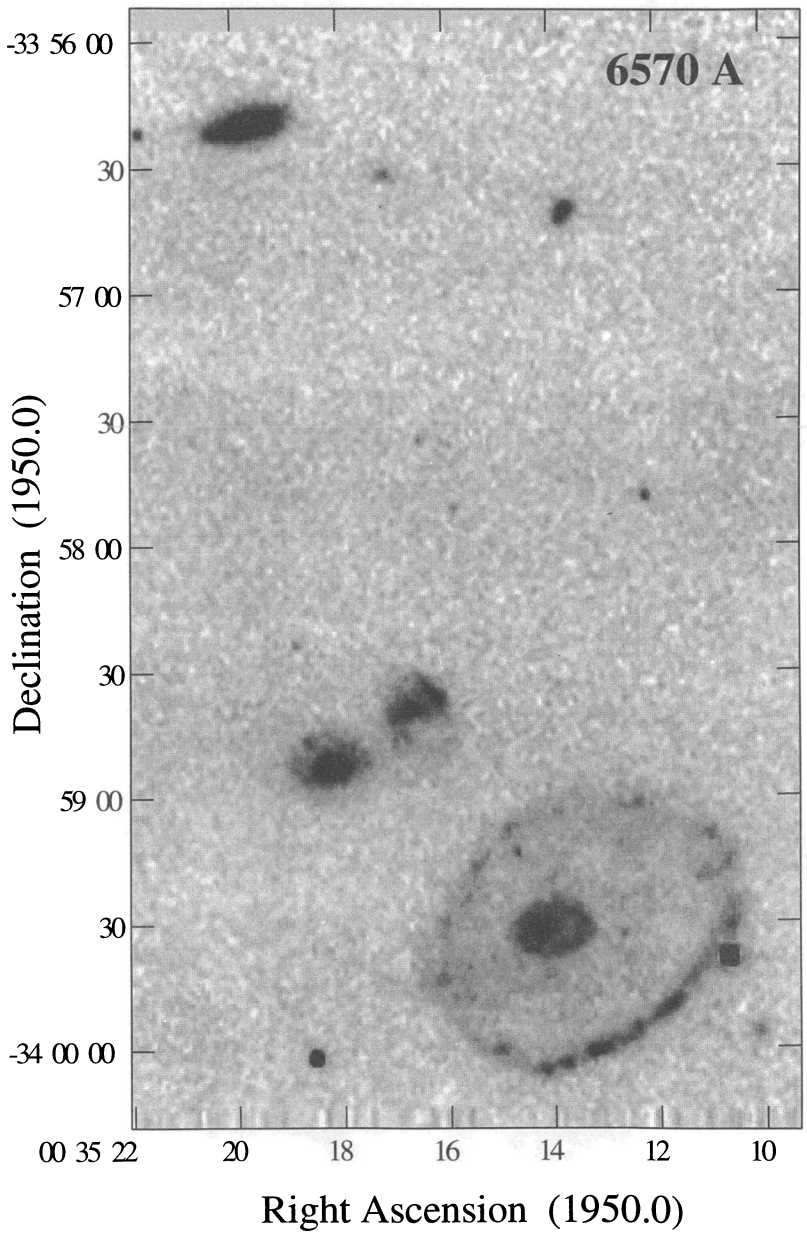

FIG. 2b

FIG. 2.—The Cartwheel Group in (*a*) Hα and (*b*) red continuum (λ = 6570 Å, $\Delta\lambda$ = 150 Å FWHM). Subimages of the full frames show (*c*) Hα and (*d*) red continuum emission from the ring. A linear transfer function has been used throughout. (*e*) Contour map of (*c*) with H II region complexes labeled. Contours are in equal increments of 2.1×10^{-15} ergs s^{-1} cm^{-2} $arcsec^{-2}$, starting at 1.0×10^{-15} ergs s^{-1} cm^{-2} $arcsec^{-2}$.

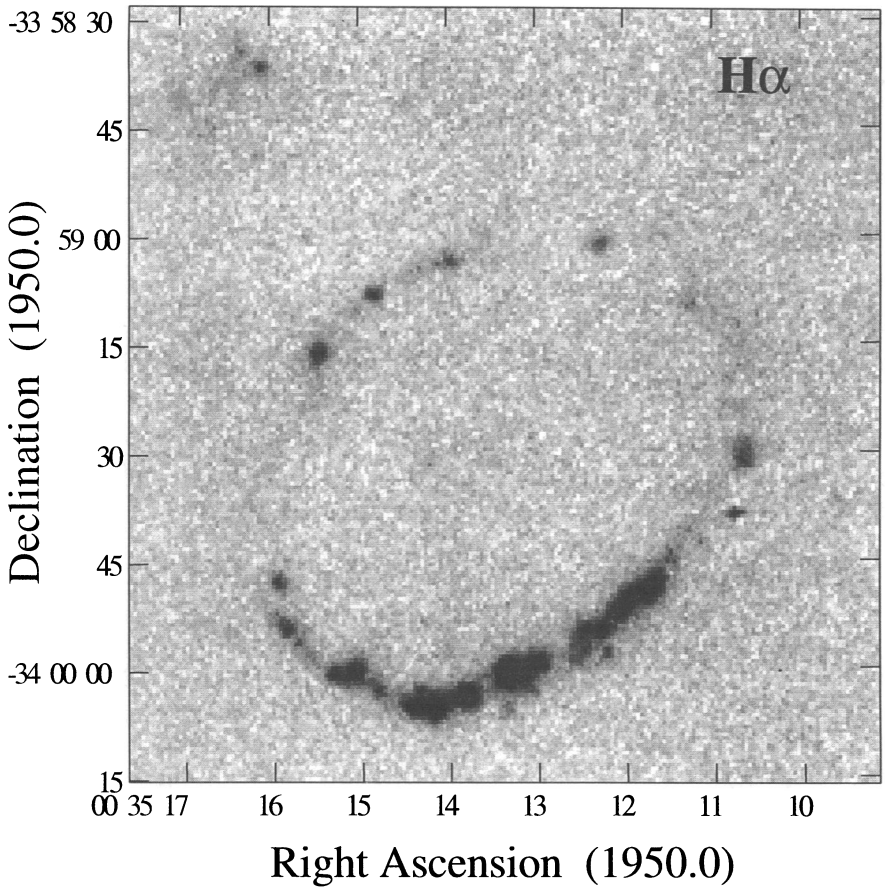

FIG. 2*c*

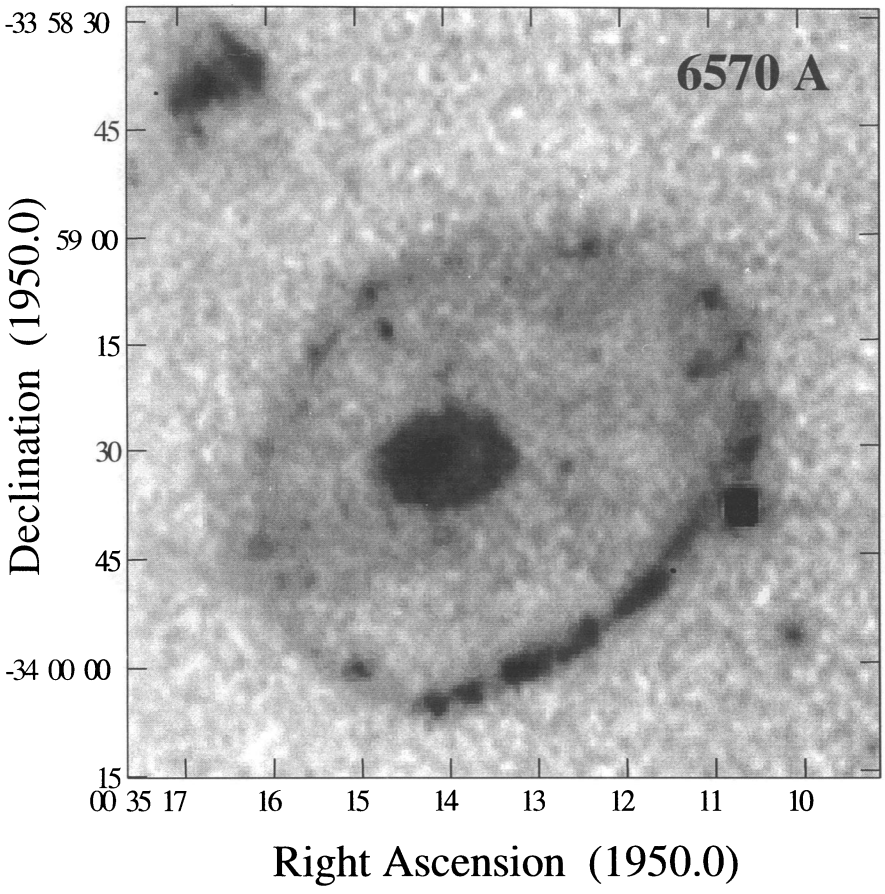

FIG. 2*d*

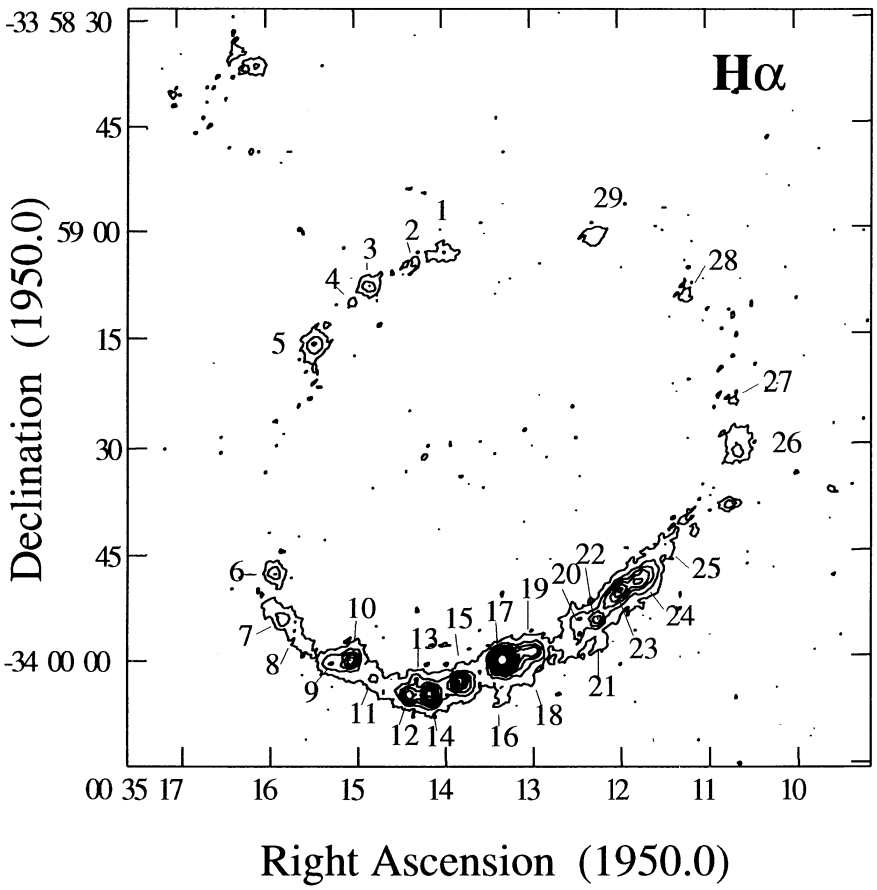

FIG. 2e

the ring in Figure 2c, though overall, the ring is well fit by an ellipse. There is no obvious radial structure in the ring's southern quadrant.

3.2. *Red Continuum Emission in the Cartwheel*

The ring galaxy emits a continuum flux at 6570 Å of 1.5×10^{-14} ergs s^{-1} cm^{-2} $Å^{-1}$. Unlike the situation with Hα in which the outer ring is totally dominant, the inner ring + bar + nucleus and outer ring contribute comparable 6570 Å fluxes. Significant differences were found between the distributions of Hα and red continuum in the outer ring of the Cartwheel. First, the azimuthally averaged profiles shown in Figure 4 show that continuum emission (*open circles*) falls off gradually with decreasing radius interior to the ring. This

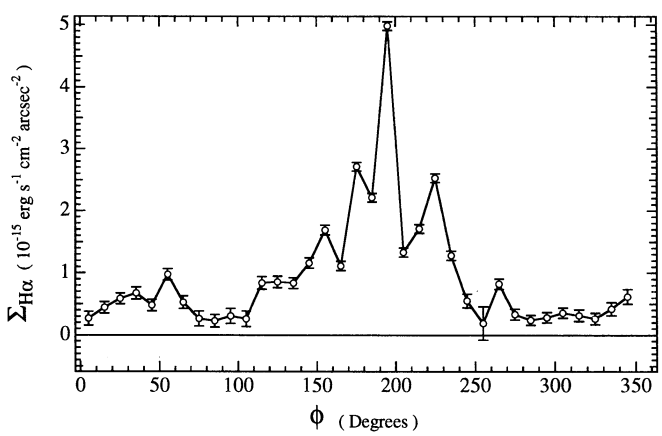

FIG. 3a

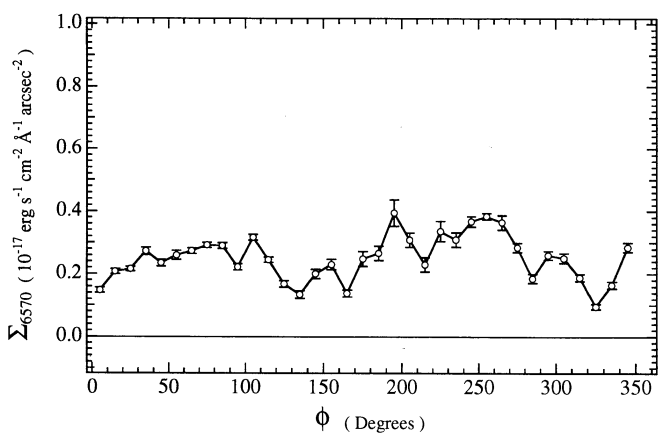

FIG. 3b

FIG. 3.—Averaged azimuthal surface brightness profiles around the outer ring. (*a*) Hα; (*b*) 6570 Å continuum. Position angle (ϕ) is measured counterclockwise from a line extending north from the ring center.

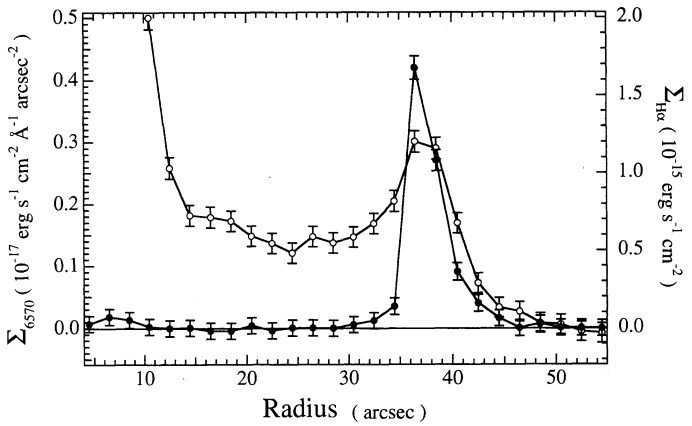

FIG. 4.—Azimuthally averaged radial surface brightness profiles in red continuum (*open circles*) and Hα (*filled circles*) for the Cartwheel. The entire range of azimuth was used to construct the averages.

radial "tail" is totally absent in the identically defined radial Hα profile (*filled circles*) in Figure 4. Line emission drops sharply on either side of the peak centered on the ring. The azimuthal variations of Hα and red continuum emission in the outer ring shown in Figure 3 reveal larger differences: while the minimum and peak Hα surface brightnesses constitute a variation of more than an order of magnitude, the red continuum surface brightness changes only by a factor of approximately 2. Red continuum peaks in two regions of the ring, i.e., $\phi = 20°$–$120°$ and $170°$–$270°$. However, these are significantly *different* from the locations of the twin peaks corresponding to the southern and northeast quadrants seen in Hα ($\phi = 0°$–$70°$ and $120°$–$250°$).

A number of prominent knots of continuum emission are found coincident with bright H II complexes in the outer ring, especially in the southern quadrant. These undoubtedly represent emission from the embedded star clusters driving the H II regions. The continuum emission *between* these knots should provide a reasonable upper limit to the strength of the underlying ring density wave. From Figure 2*d*, the mean red continuum surface brightness of the ring between H II complexes CW 15 and 17 is 3.5×10^{-18} ergs s^{-1} cm^{-2} Å^{-1} arcsec^{-2}. This is similar to surface brightnesses measured elsewhere in the ring (e.g., between H II complexes in the northeast quadrant). Moreover, there exists a large segment of the outer ring between position angle $\phi = 240°$–$310°$ in which (*a*) the red continuum surface brightness equals or exceeds 3.5×10^{-18} ergs s^{-1} cm^{-2} Å^{-1} arcsec^{-2}, and (*b*) comparatively little MSF is occurring. The factor of 2 enhancement in the southern quadrant's 6570 Å surface brightness apparent in Figure 3*b* appears to be largely caused by young stellar associations in the H II region complexes. The actual variations in the ring itself are much smaller. While the southern quadrant is clearly experiencing most of the Cartwheel's MSF, the amplitude of the underlying stellar ring, as reflected by the red continuum light, is *not* significantly different from any other part of the outer ring. The ring's stellar amplitude is not the primary factor determining MSF. A similar conclusion is reached using the inner ring. From Figure 2*d*, an average 6570 Å continuum surface brightness of 8.0×10^{-18} ergs s^{-1} cm^{-2} Å^{-1} arcsec^{-2} was measured. This is roughly twice the peak value of the outer ring (discounting H II knots). Strong orbit crowding in the rings does not appear to translate directly into MSF.

3.3. Hα *Equivalent Widths in the Outer Ring*

Because only stars more massive than $\sim 10\ M_\odot$ contribute significantly to an H II region's line luminosity, and because the bulk of the red continuum is furnished by stars of low to intermediate mass, Hα equivalent widths ($EW_{H\alpha}$) can be used to measure the relative strengths of these two populations (Sarazin 1976; Kennicutt 1983; von Hippel & Bothun 1990). While fairly insensitive to extinction, equivalent widths are strong functions of the mean age, the age spread, and initial mass function (IMF) of the star-forming regions. Metallicity may also affect EWs by modifying stellar evolution and the ionizing spectrum. However, since the Cartwheel's outer ring is nearly at the same radius and unlikely to possess large abundance gradients, this is not thought to be a major factor. The large-scale variations in $EW_{H\alpha}$ around the ring shown in Figure 5 were derived by dividing the line and continuum profiles of Figure 3. The observed dependence of $EW_{H\alpha}$ on ϕ is nearly identical to the azimuthal Hα profile. Very large values are found, especially in the ring's southern quadrant, which peaks at $EW_{H\alpha} = 1250$ Å and exceeds 400 Å everywhere. A much more modest enhancement in $EW_{H\alpha}$ corresponding to the northeast quadrant is also apparent in Figure 5. Integrated over the Cartwheel, $EW_{H\alpha} = 113 \pm 17$ Å, which is also large compared with other galaxies. Noninteracting Sb and Sc spirals possess typical $EW_{H\alpha+[N\,II]}$ values of 10 Å and 30 Å, respectively (Kennicutt 1983). The Cartwheel's $EW_{H\alpha}$ significantly exceeds median values for close pairs and strongly interacting Arp galaxies of types Sd and earlier ($EW_{H\alpha+[N\,II]} < 38$ Å; Kennicutt et al. 1987). Only types Sm – Im in these samples possess $EW_{H\alpha+[N\,II]}$ comparable to that of the Cartwheel.

3.4. *The Ring* H II *Complexes*

A total of 29 H II complexes were identified using the Hα image and are shown labeled in Figure 2*e*. Their measured emission properties and positions are listed in Table 2. The integrated Hα luminosities of these regions, even without extinction corrections, are extreme. Almost all exceed $L_{H\alpha} = 10^{40}$ ergs s^{-1}, placing them in the giant and supergiant luminosity class (Kennicutt et al. 1989). The most luminous of these (CW 17, region "A" in FH) possesses $L_{H\alpha} = 2.2 \times 10^{41}$ ergs s^{-1}, or 13% of the entire galaxy's Hα luminosity. Typical Galactic H II regions like the Orion Nebula, powered by a few OB stars, possess $L_{H\alpha} \sim 10^{37}$ ergs s^{-1}. The nearest giant H II

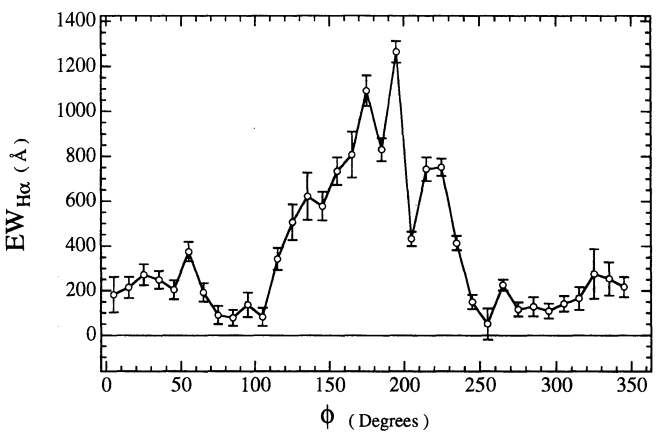

FIG. 5.—Hα equivalent widths in the Cartwheel's outer ring averaged over 10° sectors (ratio of Figs. 3*a* and 3*b*).

TABLE 2

MEASURED PROPERTIES OF CARTWHEEL H II REGION COMPLEXES

ID	ϕ	R.A.[a]	Decl.[a]	$F_{H\alpha}$[b]	$F_{6570\,A}$[c]	$EW_{H\alpha}$[d]
1.....	13	00h35m14s.04	−33°59′02″	1.87 (±0.05)	3.75 (±0.28)	3400
2.....	24	00 35 14.42	−33 59 03	1.18 (±0.05)	4.01 (±0.28)	200
3.....	35	00 35 14.90	−33 59 06	2.43 (±0.05)	6.55 (±0.30)	760
4.....	44	00 35 15.09	−33 59 08	0.63 (±0.03)	2.10 (±0.20)	1243
5.....	59	00 35 15.54	−33 59 14	4.34 (±0.07)	9.09 (±0.39)	1340
6.....	118	00 35 16.03	−33 59 44	2.56 (±0.05)	4.92 (±0.30)	1680
7.....	129	00 35 15.95	−33 59 51	3.26 (±0.06)	3.47 (±0.30)	1350
8.....	138	00 35 15.82	−33 59 52	1.59 (±0.03)	2.50 (±0.24)	5900
9.....	143	00 35 15.41	−33 59 57	3.23 (±0.05)	3.08 (±0.25)	4297
10.....	147	00 35 15.20	−33 59 56	7.08 (±0.07)	7.40 (±0.32)	1933
11.....	154	00 35 14.94	−33 59 59	2.73 (±0.05)	3.86 (±0.28)	3202
12.....	162	00 35 14.54	−34 00 01	6.61 (±0.07)	3.85 (±0.26)	5587
13.....	163	00 35 14.45	−34 00 00	1.89 (±0.04)	1.57 (±0.19)	4195
14.....	167	00 35 14.33	−34 00 02	10.72 (±0.08)	8.29 (±0.32)	2727
15.....	174	00 35 13.97	−34 00 00	10.23 (±0.08)	10.70 (±0.36)	2398
16.....	184	00 35 13.49	−34 00 02	1.30 (±0.04)	<0.88 (±0.25)	...
17.....	185	00 35 13.48	−33 59 57	33.31 (±0.14)	22.03 (±0.46)	5756
18.....	191	00 35 13.22	−33 59 59	2.36 (±0.05)	<1.32 (±0.26)	...
19.....	192	00 35 13.15	−33 59 56	7.28 (±0.07)	11.11 (±0.30)	3990
20.....	211	00 35 12.64	−33 59 52	6.48 (±0.08)	11.81 (±0.38)	4100
21.....	212	00 35 12.37	−33 59 55	1.13 (±0.08)	<0.42 (±0.19)	...
22.....	214	00 35 12.42	−33 59 52	5.08 (±0.06)	4.07 (±0.25)	4000
23.....	224	00 35 12.15	−33 59 48	10.12 (±0.09)	10.93 (±0.36)	2769
24.....	231	00 35 11.95	−33 59 47	11.02 (±0.09)	15.75 (±0.41)	1853
25.....	243	00 35 11.67	−33 59 42	1.62 (±0.04)	5.23 (±0.25)	859
26.....	271	00 35 10.79	−33 59 29	3.78 (±0.06)	12.05 (±0.35)	689
27.....	283	00 35 10.77	−33 59 23	1.02 (±0.05)	5.98 (±0.29)	387
28.....	309	00 35 11.34	−33 59 08	1.32 (±0.05)	5.76 (±0.31)	583
29.....	333	00 35 12.35	−33 59 00	1.92 (±0.06)	6.67 (±0.33)	728

[a] 1950.0 coordinates.
[b] In units of 10^{-14} ergs s^{-1} cm^{-2}.
[c] In units of 10^{-16} ergs s^{-1} cm^{-2} $Å^{-1}$.
[d] In units of Å, after subtraction of background ring emission.

region is 30 Doradus in the LMC, with $L_{H\alpha} = 6 \times 10^{39}$ ergs s^{-1}. Given the 750 pc resolution of the maps, observations made under much better seeing conditions will be required to describe the luminosity function of individual ring H II regions. Figure 6*a* shows the distribution of luminosities with ϕ for the H II region complexes in the ring. One can see that the southern quadrant is an enhancement in both their number density and luminosity. This is also true to a smaller extent in the northeast quadrant. A further indication of how the line emission is dominated by highly luminous complexes is that their combined $L_{H\alpha}$ accounts for 86% of the Cartwheel's total Hα luminosity. This is in marked contrast with M51 (Rand 1992), where the H II region complexes account for only 45% of the total line emission.

In Figure 2*c*, three comparatively low luminosity H II region complexes can be seen just beyond the outer ring in the southern quadrant (CW 16, 18, and 21). All three are found adjacent to one of the more luminous complexes. In particular, CW 16 and 18 are linked with CW 17. Figure 7 shows a slice along a line joining the peaks of CW 16 and 17 in Hα, showing

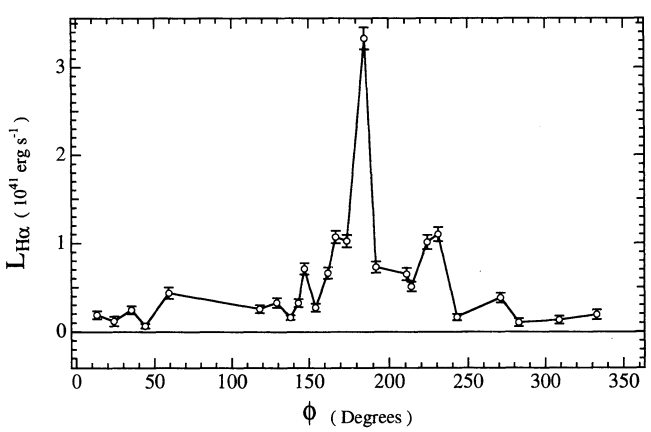

FIG. 6*a*

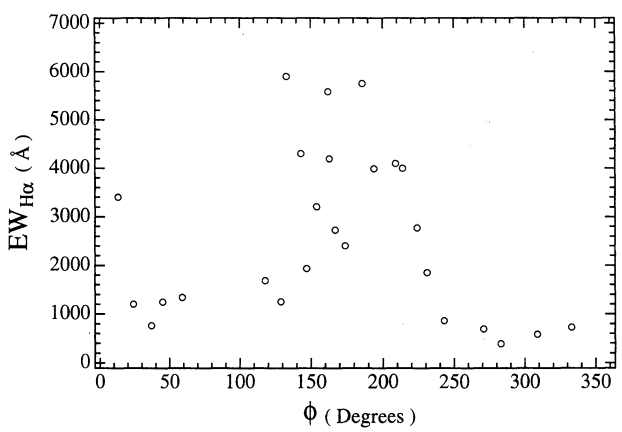

FIG. 6*b*

FIG. 6.—Emission properties of the outer ring star-forming regions as a function of position angle (ϕ). (*a*) $L_{H\alpha}$; (*b*) $EW_{H\alpha}$ after removal of the ring background.

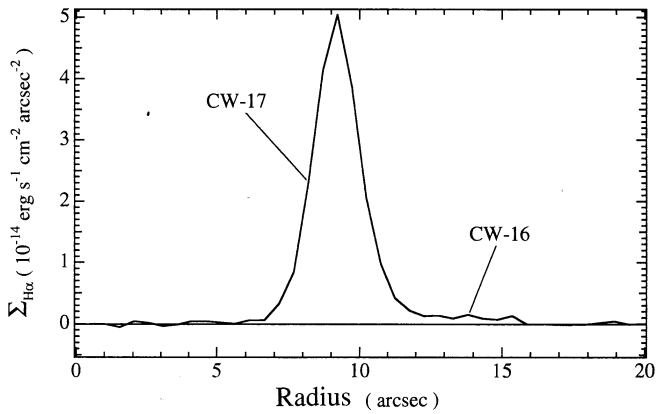

FIG. 7.—Radial slice through H II region complexes CW 16 and CW 17 in Hα, showing the faint bridge between them.

a faint emission-line bridge. It seems reasonable to interpret these features as secondary H II complexes spawned by shocks or stellar winds from the luminous star-forming regions of the ring. No such star-forming regions were found interior to the ring.

Equivalent widths of individual star-forming regions required the subtraction of the line and continuum contribution from the ring background, which was at times difficult owing to their close spacing. Reasonably accurate measurements of $EW_{H\alpha}$ were made for 24 of the Cartwheel's 29 H II complexes. These are listed in Table 2 and shown plotted against ϕ in Figure 6*b*. The same general azimuthal dependence found in the averaged azimuthal profiles (Fig. 5) is present in the H II complex population, though with considerably more scatter, largely as a result of uncertainties in the background subtraction. Still, the H II region $EW_{H\alpha}$ values are extremely large. For example, $EW_{H\alpha}$ measured in typical spiral arm H II regions range from ~100 Å to near 2000 Å, with mean values near 600 Å (von Hippel & Bothun 1990; Waller 1991). $EW_{H\alpha}$ in the Cartwheel's H II regions are 2600 Å on average, similar to values found in metal-poor starburst galaxies. Peak values are all found in the southern quadrant, where CW 12 and 17 are all close to 6000 Å. For both regions, the ring background was relatively easy to estimate and is not believed responsible for the extreme values.

4. DISCUSSION

4.1. *The Rate of Star Formation in the Cartwheel*

Using the Cartwheel's extinction corrected Hα luminosity, a massive star formation rate ($M > 10\ M_\odot$) of 11 $M_\odot$ yr^{-1} was derived (Kennicutt 1983). Similarly defined massive star SFRs for giant Sc galaxies lie between 0.4 and 0.8 $M_\odot$ yr^{-1}. If the precollision Cartwheel was a late-type spiral as suggested by Mebold, Goss, & Fosbury (1977), then the interaction has led to an increase in the global massive SFR by at least an order of magnitude, with all this activity confined to the narrow 33 kpc diameter ring. Adopting the IMF used by Kennicutt (1983) leads to a total SFR ($0.1 < M/M_\odot < 100$) of 67 $M_\odot$ yr^{-1}. Total SFRs of ~100 $M_\odot$ yr^{-1} are commonly inferred from 10 μm to 1 mm continuum fluxes of starburst galaxies (Schweizer 1987). By this definition, the Cartwheel is experiencing a moderate starburst. Over the remainder of the galaxy, an upper limit to the total SFR of 0.3 $M_\odot$ yr^{-1} (3 σ) was set. This level is comparable to that found in the disks of Sa galaxies by Caldwell et al. (1991). An estimate of the total SFR averaged over the lifetime of the Cartwheel was derived by multiplying its blue luminosity (Higdon 1995) by a late spiral M/L_B ratio (Faber & Gallagher 1979) and dividing by 15 Gyr. This resulted in $SFR_{past} = 7.4\ M_\odot$ yr^{-1}, similar to values derived in other disk systems (Caldwell et al. 1991; Kennicutt 1983). Star formation in the Cartwheel has clearly been enhanced by the interaction, as can be seen from the ratio of SFR/SFR_{past}, which is 9 for the ring galaxy. This quantity increases with galaxy type, and is in the range 0.4–2 for Sbc-Sc-Sd galaxies (Kennicutt 1983). Since the Cartwheel's M/L_B could conceivably be much smaller, and because roughly half the L_B originates in the outer ring, the enhancement in MSF could well be even greater. As a further example of the extreme nature of MSF in the Cartwheel's ring, note that Melnick, Terlevich, & Eggleton (1985) define violent star-forming regions (VSFRs) to be small (~300 pc) regions in which several thousand massive stars are formed over a few Myr. Such regions would have massive SFR/area of $\sim 2 \times 10^{-7}\ M_\odot$ yr^{-1} pc^{-2}. Almost all the southern quadrant H II regions satisfy this definition. Even CW 5 of the comparatively quiescent northeast quadrant approaches this level of activity. The Cartwheel's outer ring can therefore be thought of as a highly extended VSFR, one nearly 100 kpc in circumference.

4.2. *Gas in the Inner Ring and Spokes*

The lack of MSF in the Cartwheel's inner ring and spokes argues that they are not gas rich. The strong orbit crowding in the inner ring implied by the large $\Sigma_{6570\,Å}$ (~2 times that of the outer ring) would be expected to produce high gas surface densities and detectable levels of Hα emission unless this region of the disk were largely free of atomic or molecular gas. Similarly, the spokes represent significant enhancements in optical surface density over the rest of the disk, and ring galaxy models have concluded that high gas surface densities in the spokes, comparable even to the outer ring, are required to generate spokes which are as sharply defined and prominent as the Cartwheel's (Hernquist & Weil 1993). If so, one might expect similarly high levels of MSF, which is not seen. Either ring galaxies can form sharply defined spokes without a dense gas component, or other factors are suppressing MSF in them.

While the spokes and inner ring clearly represent enhancements in the stellar surface density, they do not appear to be strong enhancements in the gas surface density. Instead, the distribution of MSF points to the outer ring as being the primary reservoir of gas in the system.

4.3. *Triggered Star Formation in the Ring*

The basic motion of stars and gas clouds in a ring galaxy are epicyclic, and stars currently taking part in the ring's expansion will eventually return to smaller radii. The fact that no Hα emission is seen interior to the ring has an interesting consequence for star formation. Unless the entire Cartwheel gas supply is totally locked up in this narrow structure, this means that essentially no stars massive enough to power prominent H II regions exist outside of the ring. The simplest explanation for this is that stars born in the ring remain there longer than the main-sequence lifetime of a B5 V star (~40 Myr). Individual gas clouds should stay in the ring for at least as long. This 40 Myr timescale is similar to estimates of the growth time of giant molecular cloud complexes in spiral galaxies. The clear implication is that the ring is capable of concentrating the Cartwheel's ISM in a narrow region long enough to promote the growth of massive clouds. Does it also directly trigger star

formation as well? Or do spontaneous star formation processes dominate? Note that if by triggering, one means induced to occur where it has not previously (Elmegreen 1992), then the Cartwheel's outer ring is clearly a star formation trigger: the combination of high SFR with low metal abundances points to this being the first major episode of MSF at this radius in the Cartwheel's disk. Evidence for the *direct* triggering of MSF can be found in the observed variations in $L_{H\alpha}$ and $EW_{H\alpha}$ around the outer ring. Since both quantities are highly age dependent, a random superposition of many star-forming events around the ring, each with different rates of star formation and ages, would not be expected to produce such an ordered distribution. One could also suppose that the ring acts merely to organize the ISM into a ring, with spontaneous star formation in one segment leading to a "wave" of propagating MSF around the gas ring (Gerola & Seiden 1978). However, such an occurrence would produce a ramp-shaped distribution in $L_{H\alpha}$ and $EW_{H\alpha}$, rather than the symmetric and peaked profiles seen in Figures 3*a* and 5*a*.

The observed distribution of MSF instead bears a strong resemblance to that produced in hydrodynamic models of ring galaxies formed in a small impact parameter intruder passage (Appleton & Struck-Marcell 1987b). These crescent-shaped rings show systematic changes in the strength of orbit crowding with position angle. Because regions of peak gas density also possess the highest cloud collision rates and speeds in these models, the resulting intensity of star formation shows a similar crescent-shaped distribution. This comparison is strengthened by the presence of an extended region of depressed surface brightness seen just interior to the southern quadrant, visible in Figure 1. This band can be interpreted as a region of strong rarefaction arising from stars streaming out of the ring to smaller radii (Marcum, Appleton, & Higdon 1992). The hydrodynamic models show that these rarefaction regions are found adjacent to regions of the rings experiencing the strongest orbit crowding. The clear association of the dark band with the segment of the ring possessing the greatest Hα emission is evidence that regions of peak MSF are also regions of peak density and orbit crowding in the ring. A plausible mechanism for star formation triggering is through enhanced cloud collision rates, possibly reducing the time required to build clouds to a critical mass through the merging of smaller clouds, or by hastening their collapse through collisions.

The detection of faint secondary H II regions only in advance of the outer ring can be explained as the result of MSF triggered near the outer edge of a gas-rich ring. If the giant H II region complexes of the southern quadrant were embedded in the middle of a gas ring, they would be expected to be capable of spawning H II regions both behind and ahead of the ring. Star formation triggered preferentially to the ring's leading edge would allow stellar winds and shocks to break out into the less dense gaseous environment beyond the ring. The envisioned situation is similar to the starburst-driven superwinds escaping into the halo from the disks of FIR luminous galaxies (Heckman, Armus, & Miley 1990). It should also be noted that the hydrodynamic models of Appleton & Struck-Marcell (1987b) predict that MSF will occur preferentially near the ring's outer edge, since this is where cloud agglomeration is greatest.

4.4. *Are There Systematic SFR, Age, or IMF Variations?*

Previous sections have shown that systematic variations exist in the $L_{H\alpha}$ and $EW_{H\alpha}$ of the Cartwheel's star-forming regions, both when averaged over 10° sectors and when individual H II region complexes are considered. Both quantities peak in the southern quadrant. One finds a higher concentration of star-forming complexes there as well. What process is primarily responsible for these observed trends? One possibility involves changes in the local rate of MSF around the outer ring. The peaking of $L_{H\alpha}$ in the southern quadrant would simply require that more massive stars are being formed per unit time than other stretches of the ring. However, this interpretation is at odds with the observed azimuthal dependence in $EW_{H\alpha}$, which indicates changes in stellar populations. Two ways to achieve this are through differences in age or IMF. Since the stars most responsible for large $L_{H\alpha}$ and $EW_{H\alpha}$ are also the shortest lived, small age differences between two star-forming regions can produce sizable differences in observed emission properties. For example, models of low-metallicity H II regions show that for a standard IMF, $EW_{H\beta}$ decreases by a factor of 2 in only 10 Myr (Olofsson 1989). Similar time dependence is expected in $EW_{H\alpha}$. This leads to the "aging ring" interpretation, where the *ages* of star-forming regions increase progressively away from the southern quadrant, where the youngest are concentrated. There are a few problems with this hypothesis. The first is presented by the presence of strong radial color gradients in the optical and near-infrared through the Cartwheel's disk (Marcum et al. 1992). The ring has been forming stars continuously throughout its ~300 Myr march outward. Why then do we not find older star-forming regions, with much smaller $L_{H\alpha}$ and $EW_{H\alpha}$, mixed in with the young through the southern quadrant? For that matter, why does one not see young H II region complexes in other parts of the ring? Second, it is not clear from the available ring galaxy simulations that the required distribution of ages would come about.

Alternately, the population differences implied by the $EW_{H\alpha}$ could be caused by systematic changes in the IMF among a collection of coeval star-forming regions. The southern quadrant in this case represents a region where either the IMF slope or upper mass limit (or both) has peaked. While it was unclear how systematic age differences could arise from variations in the properties of the expanding ring, changes in the IMF are easier to conceive. The models of Appleton & Struck-Marcell (1987b) predict that the region of peak gas density will also be where the cloud collision speed and frequency are the greatest. High collision speeds between clouds has been proposed as a way to affect their mass spectrum by preferentially destroying low-mass clouds (Elmegreen 1992). At the same time, increased cloud collision rates would promote the growth of larger cloud complexes, which would result in more massive stars. Once star formation has begun, feedback from the concentrated star-forming regions (e.g., local heating of the ISM or turbulence from supernova shocks) would disrupt low-mass clouds or raise the Jeans mass, both effects tending to retard the formation of lower mass stars. These combined effects lead to the following possible sequence of events: A small but nonzero impact parameter intruder passage creates an outwardly moving crescent-shaped ring. The rate of MSF is greatest at the site of the gas density peak, where more frequent and violent collisions between clouds create very massive cloud complexes and trigger their collapse. Initially, the SFR varies much like density around the ring. Feedback effects arise which favor the formation of massive stars (or the suppression of low-mass stars), either through the destructive effects of massive stars or through cloud collision speeds. The result is

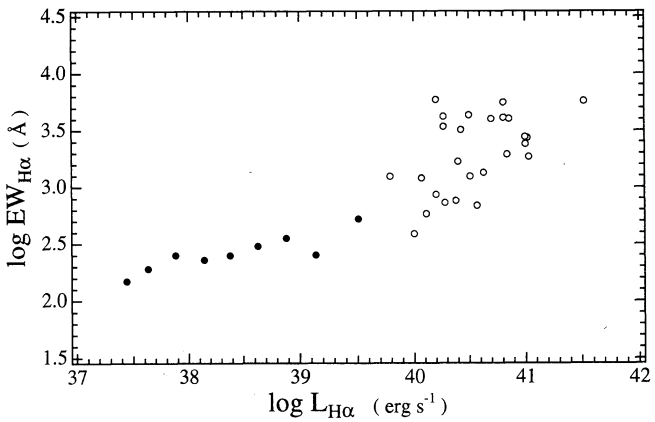

FIG. 8.—Star-forming region $EW_{H\alpha}$ as a function of $L_{H\alpha}$ for NGC 628 (*filled circles*; von Hippel & Bothun 1990) and the Cartwheel (*open circles*).

azimuthal variations in the IMF that could account for the observed $L_{H\alpha}$ and $EW_{H\alpha}$ variations.

Apart from possible azimuthal changes in stellar populations around the ring, are there any indications of an IMF biased toward massive stars in the Cartwheel? Figure 8 shows a comparison between $L_{H\alpha}$ and $EW_{H\alpha}$ for the H II region populations of NGC 628 (von Hippel & Bothun 1990) and the Cartwheel. For both sets, the background line and continuum contributions have been subtracted. Each is well represented by power laws of the form $EW_{H\alpha} = a(L_{H\alpha})^b$. Least-squares fits show that the Cartwheel's H II complexes possess a significantly greater exponent ($b_{Cartwheel} = 0.83 \pm 0.10$, versus $b_{NGC\,628} = 0.23 \pm 0.05$), meaning that the Cartwheel H II regions possess systematically greater $EW_{H\alpha}$ for a given Hα luminosity. Since $EW_{H\alpha}$ measures the relative strengths of the high- and low-mass stellar populations, this result is consistent with an enhanced upper end of the Cartwheel's IMF relative to NGC 628. A subsequent paper will address the changes in the IMF and ages required to account for these differences.

Despite observations suggesting peculiar IMFs in galaxies, proof has remained elusive, primarily because of the difficulty in distinguishing age and IMF effects. It is hoped that new and better diagnostics of star-forming regions, such as the analysis of optical and near-infrared absorption features, will lead to less ambiguous determinations of ages and populations. Detailed numerical modeling of the history of star formation in ring galaxies is also eagerly awaited.

4.5. *Star Formation in the Companion Galaxies*

Table 3 lists the integrated Hα and 6570 Å continuum fluxes from the Cartwheel's three companion galaxies. Each contributes much lower levels of emission than the ring galaxy. Line emission from the companions is more diffuse and is not dominated by star-forming regions, as is the case in the Cartwheel. In fact, the brightest H II complexes in G1 and G3 would be among the faintest of the ring's population. Total star formation rates using each galaxy's Hα fluxes are also listed in Table 3 and are both $\sim 2\ M_\odot\ yr^{-1}$. These are somewhat higher than typically seen in small spirals. G1 possesses the largest $EW_{H\alpha}$ of the three (31 ± 5 Å) but is still considerably smaller than the Cartwheel's. For G1 and G3, $EW_{H\alpha}$ is still large compared with Kennicutt's (1983) sample of spiral galaxies.

Which of the three is responsible for the ring's formation is still uncertain. Since tidal interactions clearly lead to enhanced MSF in spirals, it was hoped that the intruder would be "fingered" by its own starburst activity. Jeske (1986) found a strong tendency for enhanced MSF in companion galaxies that can be unambiguously identified as intruders. However, all three intruder candidates show evidence of tidal interactions at some level in Figure 1. For example, G1 possesses peculiar spiral arms, while G2 shows evidence of a faint tidal plume extending to the north, in addition to a noticeably off-centered core. Further evidence of recent tidal interactions can be found in the enhanced SFR and $EW_{H\alpha}$ of G1 and G3.

5. CONCLUSIONS

Hα and red continuum CCD surface photometry of the Cartwheel Group has been obtained with the goals of mapping the intensity and distribution of massive star formation in the ring galaxy and determining basic properties of the ring H II region complexes. The results of this study are as follows:

1. Massive star formation is totally restricted to the Cartwheel's outer ring, where an integrated Hα luminosity of 1.7×10^{42} ergs s^{-1} has been measured with no extinction correction. There is no evidence of massive star formation (MSF) in the ring galaxy's nucleus, inner ring, disk, and spokes above a smoothed Hα surface brightness of 2.6×10^{31} ergs s^{-1} pc^{-2} (3 σ), a value half of what would be expected from the faint interarm region of M51. Applying an average extinction correction ($A_{H\alpha} = 1.6$), $L_{H\alpha} = 7.4 \times 10^{42}$ ergs s^{-1}.

2. Line intensity varies systematically around the outer ring and peaks in one quadrant (southern quadrant). More than 80% of the Cartwheel's total $L_{H\alpha}$ and two-thirds of its H II

TABLE 3

INTEGRATED EMISSION PROPERTIES

Galaxy	$F_{H\alpha}$[a]	$F_{6570\,A}$[b]	EW_{tot}[c]	$L_{H\alpha}$[d]	SFR[e]	R[f]
Cartwheel.....	1.7×10^{-12}	1.5×10^{-14}	113 ± 17	7.4×10^{42}	67	9.1
G1.....	4.0×10^{-14}	1.3×10^{-15}	31 ± 5	1.8×10^{41}	1.7	0.4
G2.....	...	2.4×10^{-15}	...	...	...	...
G3.....	5.4×10^{-14}	2.3×10^{-15}	24 ± 5	2.4×10^{41}	2.2	0.9

[a] In units of ergs s^{-1} cm^{-2}.
[b] In units of ergs s^{-1} cm^{-2} Å^{-1}.
[c] In units of Å.
[d] In units of ergs s^{-1} at the assumed distance of 91 Mpc. A mean $A_{H\alpha} = 1.6$ mag has been applied to each galaxy's Hα flux.
[e] Assuming a Miller-Scalo IMF with stellar masses ranging over $0.1 \leq M/M_\odot \leq 100$ (Kennicutt 1983).
[f] $R = SFR/SFR_{15\,Gyr}$.

region complexes are found here. Similar azimuthal variations are seen in $EW_{H\alpha}$, which also show extreme values.

3. Luminous knots that correspond to the giant H II region complexes are seen in the red continuum map. Assuming that the emission between these knots provides an upper limit to the strength of the underlying ring density wave, there are surprisingly weak variations around the outer ring. There is no direct correspondence between the stellar amplitude of the outer ring and strength of MSF. The red continuum surface brightness of the inner ring generally exceeds that of the outer ring.

4. Eighty-five percent of the measured Hα emission originates in 29 H II region complexes, most of which possess $L_{H\alpha} > 10^{40}$ ergs s^{-1}. A fainter distribution of line emission fills the space between the H II region complexes and completes the ring. Extreme $EW_{H\alpha}$ are also measured. Large and systematic azimuthal variations are again indicated. Three fainter star-forming regions are seen in advance of the outer ring. Their close association with luminous ring H II regions (in two cases, Hα bridges are present) implies that they have been spawned by shocks or stellar winds "breaking out" from the outer ring.

5. The large derived total star formation rate (67 $M_\odot$ yr^{-1}) and large current-to-past SFR ratio (>9) show that the Cartwheel is experiencing a starburst, with all the activity restricted to the 33 kpc diameter outer ring. The distribution of MSF in the ring is very similar to that of gas density in model rings formed in slightly off-centered collisions with a companion galaxy.

6. The systematic variations in $L_{H\alpha}$ and $EW_{H\alpha}$ indicate direct MSF triggering by the ring. The high SFR and low metallicities present in the ring imply that the ring is triggering the first major episode of star formation at this radius. The lack of secondary H II region complexes *interior* to the ring implies that MSF is being triggered on the outer edge of a gas ring.

7. The lack of MSF interior to the ring is likely the result of an overall reduction in gas density, possibly below a critical threshold for star formation. Most of the ISM probably resides in the outer ring. Since strong orbit crowding is apparent in the Cartwheel's inner ring, the lack of MSF there likely reflects a lack of gas. Finally, the spokes cannot be gas rich, certainly not on a par with the outer ring.

8. The systematic changes in $L_{H\alpha}$ and $EW_{H\alpha}$ are consistent with either age or IMF variations around the ring, but not SFR variations. It is not clear how the required age variations would come about in the evolving ring. Cloud-fluid ring galaxy models do produce systematic variations around the ring in the speed and frequency of cloud collisions and density that are similar with the observed line emission. It is suggested that this may lead to strong azimuthal variations in the cloud mass spectrum, and eventually, the IMF. The Cartwheel's star-forming region population possesses greater $EW_{H\alpha}$ at a given $L_{H\alpha}$ compared with those of NGC 628, suggesting an IMF biased toward massive stars.

9. The three companion galaxies are characterized by much smaller total $L_{H\alpha}$ and $EW_{H\alpha}$. Their star-forming regions are also less extreme. All show some evidence of a recent tidal interactions. The identity of the "intruder" galaxy is still uncertain.

It is a pleasure to thank Frank Bash, Curt Struck-Marcell, Beverly Smith, Richard Rand, Keith Thompson, John Scalo, Steve Lord, and John Wallin for their comments. I also wish to thank Marshall McCall and Ed Carder (NOAO) for the use of their interference filters, and Don Taylor for assisting with the observations. A special word of thanks goes out to the staff of the McDonald Observatory, in particular Jerry Martin, Paul Greybeal, Ed Dutchover, and Martin Villareal, for keeping the telescopes, CCDs, and computers in good working order. Finally, I wish to thank Robert Kennicutt for suggesting substantial improvements in this paper.

REFERENCES

Appleton, P. N., & Struck-Marcell, C. 1987a, ApJ, 312, 566
———. 1987b, ApJ, 318, 103
Bessel, M. S. 1979, PASP, 91, 589
Caldwell, N., Kennicutt, R. C., Phillips, A. C., & Schommer, R. A. 1991, ApJ, 370, 526
de Vaucouleurs, G., de Vaucouleurs, A., Corwin, H. G., Buta, R. J., Paturel, G., & Fouque, P. 1991, Third Reference Catalog of Bright Galaxies (Berlin: Springer-Verlag)
Elmegreen, B. G. 1992, in Star Formation in Stellar Systems, ed. G. Tenorio-Tagle, M. Prieto, & F. Sánchez (Cambridge: Cambridge Univ. Press), 381
Faber, S., & Gallagher, J. 1979, ARA&A, 17, 135
Few, J. M. A., Madore, B. F., & Arp, H. J. 1982, MNRAS, 199, 633
Fosbury, R. A. E., & Hawarden, T. G. 1977, MNRAS, 178, 473 (FH)
Gerola, H., & Seiden, P. E. 1978, ApJ, 223, 129
Heckman, T. M., Armus, L., & Miley, G. K. 1990, ApJS, 74, 833
Hernquist, L., & Weil, L. 1993, MNRAS, 261, 804
Higdon, J. L. 1995, in preparation
Jeske, N. A. 1986, Ph.D. thesis, Univ. California, Berkeley
Kennicutt, R. C. 1983, ApJ, 272, 54
———. 1989, ApJ, 344, 685
Kennicutt, R. C., Edgar, B. K., & Hodge, P. W. 1989, ApJ, 337, 761
Kennicutt, R. C., Keel, W. C., van der Hulst, J. M., Hummel, E., & Roettiger, K. A. 1987, AJ, 93, 1011
Lynds, R., & Toomre, A. 1976, ApJ, 209, 382
Marcum, P. M., Appleton, P. N., & Higdon, J. L. 1992, ApJ, 399, 57
Mebold, U., Goss, W. M., & Fosbury, R. A. E. 1977, MNRAS, 180, 11P
Melnick, J., Terlevich, R., & Eggleton, P. 1985, MNRAS, 216, 255
Olofsson, K. 1989, A&AS, 80, 317
Rand, R. J. 1992, AJ, 103, 815
Sarazin, C. L. 1976, ApJ, 208, 323
Savage, B. D., & Mathis, J. S. 1979, ARA&A, 17, 73
Schweizer, F. 1987, in Nearly Normal Galaxies, ed. S. M. Faber (New York: Springer-Verlag), 18
Struck-Marcell, C., & Higdon, J. L. 1993, ApJ, 411, 108
Taylor, K., & Atherton, P. D. 1984, MNRAS, 208, 601
Theys, J. C., & Spiegel, E. A. 1976, ApJ, 208, 650
———. 1977, ApJ, 212, 616
von Hippel, T., & Bothun, G. 1990, AJ, 100, 403
Waller, W. H. 1991, ApJ, 370, 144